DOI: 10.1002/chem.200700521

Supported Bilayer Lipid Membrane Arrays on Photopatterned Self-Assembled Monolayers

Xiaojun Han,[a] Singh N. D. Pradeep,[b] Kevin Critchley,[a] Khizar Sheikh,[a] Richard J. Bushby,[b] and Stephen D. Evans*[a]

Abstract: This work demonstrates the use of photocleavable cholesterol derivatives to create supported bilayer lipid membrane arrays on silica. The photocleavable cholesteryl tether is attached to the surface by using the reaction of an amine-functionalized self-assembled monolayer (SAM) and the *N*-hydroxysuccinimide-based reagent **9**. The resultant SAM contains an *ortho*-nitrobenzyl residue that can be cleaved by photolysis by using soft (365 nm) UV light regenerating the original amine surface, and which can be patterned using a mask. The photoreaction yield was $\approx 75\,\%$ which was significantly higher than previously found for related *ortho*-nitrobenzyl photochemistry on gold substrates. The SAMs were characterized by means of contact angle measurements, ellipsometry and X-ray photoelectron spectroscopy. Patterned surfaces were characterized with SEM and AFM. After immersing the patterned surface into a solution containing small unilamellar vesicles of egg phosphatidylcholine (PC), supported lipid membranes were formed comprised of lipid bilayer over the amine functionalized "hydrophilic" regions and lipid monolayer over the cholesteryl "hydrophobic" regions. This was confirmed by fluorescence microscopy and AFM. FRAP studies yielded a lateral diffusion coefficient for the probe molecule of $0.14 \pm 0.05\ \mu m^2 s^{-1}$ in the bilayer regions and $\approx 0.01\ \mu m^2 s^{-1}$ in the monolayer regions. This order of magnitude difference in diffusion coefficients effectively serves to isolate the bilayer regions from one another, thus creating a bilayer array.

Keywords: lipid bilayers · photopatterning · self-assembly · vesicles

Introduction

Phospholipid bilayers are a critical component of all cell-based biological systems, forming both the barrier between the cytosol and the cell's exterior as well as forming the subcompartments within cells. Furthermore, the membrane proteins within the lipid bilayer serve to control cell signalling, the transfer of metabolites and waste products, and the cellular response to a range of external factors. The importance of these bilayer systems has made the formation of "artificial" membranes an important target for many years, both as freely suspended membranes[1,2] and more recently as solid supported bilayer lipid membranes (sBLMs).[3–13] It is hoped that such sBLMs will be prove suitable membrane mimics to find application in membrane-based biosensing[14–17] and drug discovery.[18] With such applications in mind there has been significant interest in the development of patterned sBLMs. A variety of approaches have been used, to date, including: 1) the creation of macroscopic, 3D, barriers to confine lipid bilayers to discrete areas;[19–24] 2) the polymerization of diacetylene containing lipids to create stable corals that could be filled with phospholipids;[25,26] 3) the direct UV irradiation (184–257 nm) of preformed sBLM through a photomask[27,28] where the exposed lipids were photodecomposed while the unexposed lipids remained fluid; 4) the patterning of self-assembled monolayer (SAM) anchor layers on gold to create regions of "fluid" phospholipid bilayer separated by regions of essentially "immobile" adsorbed lipid monolayer. In our earlier work we used microcontact printing (μCP) of cholesterol derivatives followed by "backfilling" with short-chain hydroxy terminated thiols to create the patterned SAMs, and it was found that as long as the hydroxylated region was not too large vesicles would adsorb, rupture and spread over the surface to yield bilayers

[a] Dr. X. Han, Dr. K. Critchley, Dr. K. Sheikh, Prof. S. D. Evans
School of Physics and Astronomy, University of Leeds
Leeds, LS2 9JT (UK)
Fax: (+44) 113-343-3900
E-mail: s.d.evans@leeds.ac.uk

[b] Dr. S. N. D. Pradeep, Prof. R. J. Bushby
Self-Organising Molecular Systems (SOMS) Centre
University of Leeds, Leeds, LS2 9JT (UK)

Supporting information for this article is available on the WWW under http://www.chemeurj.org/ or from the author.

above the hydroxylated regions of the surface and monolayers above the cholesterol regions of the surface.[29,30] More recently we have introduced a variation on this approach by using photocleavable fluorocarbon molecules to form hydrophobic SAMs on gold substrates. Upon irradiation, through a mask, it was possible to cleave the fluorocarbon derivatives to leave hydrophilic patches separated by hydrophobic regions.[31] These systems behaved in a similar fashion to the μCP systems mentioned above.

In this paper, we introduce some important variations on this approach. Firstly, we introduce a simple tethering system that is designed to work on both gold and silicon oxide based systems. Silicon oxide surfaces are important since they allow the use of complementary techniques, such as fluorescence microscopy, which is not possible on gold due to quenching. Secondly, rather than using the fluorocarbon derivative, as in our previous study on gold, we now introduce a cholesterol derivative since these are known to insert into the lipid layer and have proved successful in previous studies on the tethering of lipid bilayer membranes.[13,29,30,32–34]

Results and Discussion

In comparison with our previous studies[31] the introduction of *N*-hydroxysuccinimide chemistry, shown in Figure 1, introduces an additional SAM-functionalisation step. This, however, brings the advantage that the same reagents can be used to form photocleavable SAMs on metallic or oxide surfaces. The synthesis of the reagent **9** is shown in outline in Scheme 1 (see also Experimental Section) and is straightforward. Because of the susceptibility of the cholesteryl nucleus to attack by NO_2^+, it was necessary to introduce the cholesteryl group after the introduction of the 2-nitro group; hence the need for the amine protection and deprotection steps.

APMES (3-aminopropyldimethylethoxysilane) was used to form amine-terminated SAMs (Figure 1a). Ellipsometry of the APMES layer yielded an average thickness value of 7 ± 1 Å (Table 1) over five samples which is in agreement with that expected from molecular models 7 Å and to the value reported by Moon et al., 7 Å.[35] The advancing and receding water contact angles were $78\pm1°$ and $32\pm1°$ (averaged over five samples), respectively. XPS of the N 1s region showed two peaks (Figure 2) at 400.4 and 402.3 eV (Table 2), which are associated with the amine nitrogen (NH_2) and ammonium nitrogen (NH_3^+), respectively.[36–38] From the integrated intensities we estimate that ≈40% of the amine groups are protonated, which is comparable to 43% protonation reported by Kowalcyk.[39]

Reaction of the APMES SAM with the reagent **9** gave rise to a 12 ± 2 Å increase in thickness and the appearance of a new peak at 406.6 eV (Figure 2b) in the XPS spectrum associated with the NO_2 group of the tether.[40,41] After the reaction the water contact angles increased from 78 to 101° for the advancing contact angle and from 32 to 58° for the

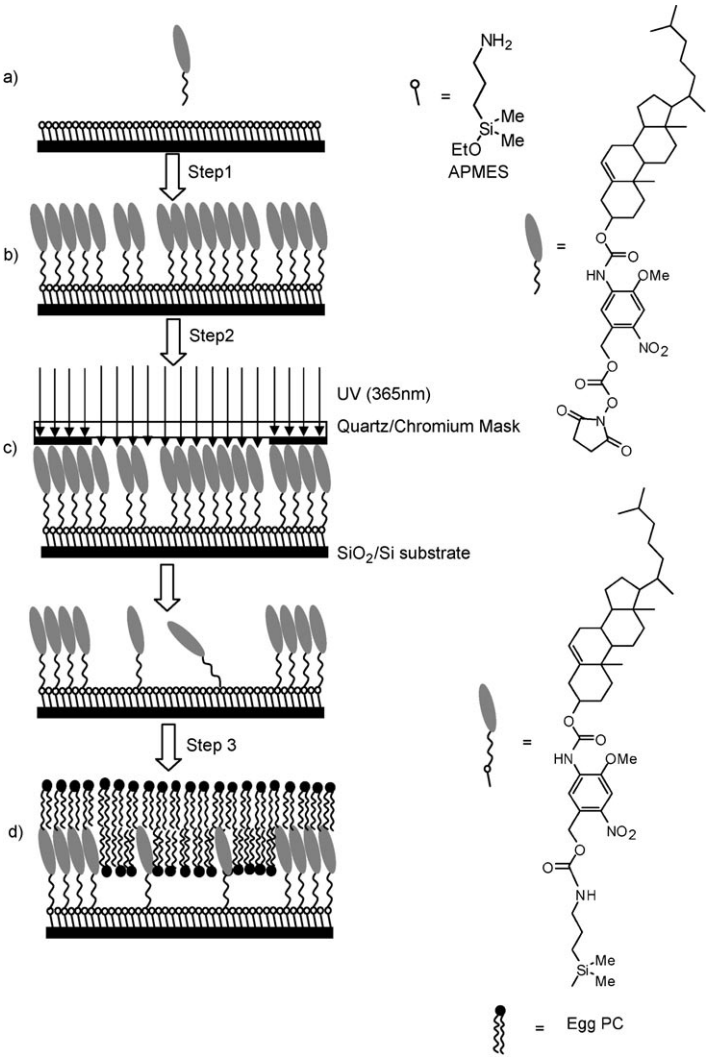

Figure 1. Schematic of the fabrication steps required to form a patterned lipid bilayer on silica surface.

receding contact angles. The significant hysteresis suggests that the water penetrated into the film or that the film is heterogeneous. From molecular models we would expect the increase in thickness to be 20 Å for a tightly-packed layer. However, the change in ellipsometric thickness of 12 Å was 60% of this value. Further from the integrated intensity of the NO_2 peak we estimate the reaction yield to be ≈50%.[42] The ellipsometry and XPS analysis suggests that the reaction is sterically hindered due to the larger cross-section area of the cholesterol molecules and the nitrobenzyl aromatic ring in comparison to the alkyl chains associated with the APMES.

Soft UV photopatterning: The *ortho*-nitrobenzyl moiety can be cleaved using 365 nm UV light.[43–47] Figure 3 shows the variation of the water contact angle as a function of irradiation time. It is evident that the limiting values obtained after prolonged irradiation (Table 1) were higher than those of the "freshly" prepared APMES SAM indicating that the re-

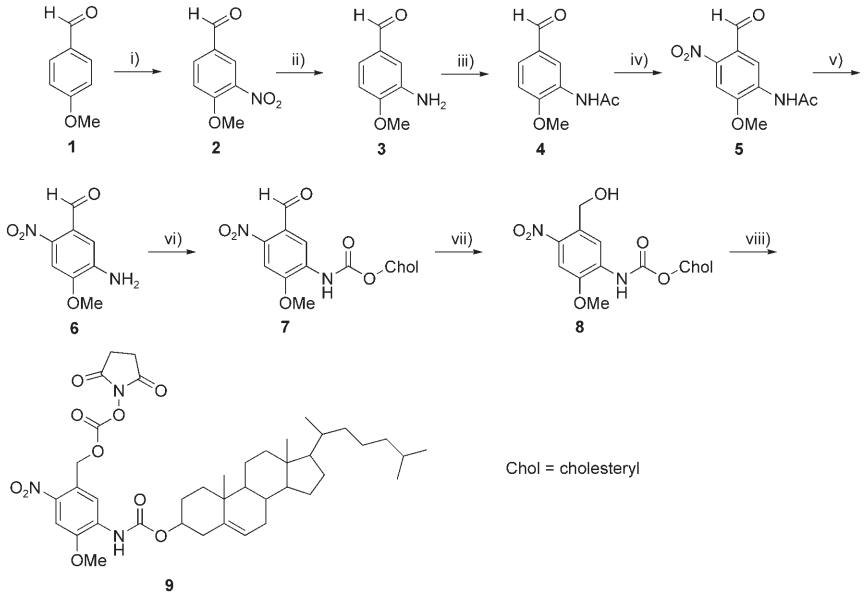

Scheme 1. Synthesis of the photocleavable tether **9**. i) 70% HNO_3, 90%; ii) Raney Ni/NH_4Cl/H_2O, 80%; iii)acetic anhydride/acetic acid, 95%; iv) 70% HNO_3, 75%; v) 2 N HCl, 70%; vi) cholesteryl chloroformate/diisopropylethylamine/DMAP/toluene, 55%; vii) $NaBH_4$/THF, 90%; viii) *N*,*N*′-disuccinimidyl carbonate/triethylamine/DMF, 85%. ^1H and ^{13}C NMR Spectra of compounds **3–9** are available in the Supporting Information.

molecules **10** have undergone a competitive side reaction and remain attached to the surface.[32,48] As shown in Scheme 2 the probable cause is a competitive photoreduction of **10** to **12**. The final film thickness following prolonged exposure was 10 ± 1 Å, that is, 3 Å greater than that of the initial APMES layer, and also consistent with $\approx$25% of **12** remaining bound to the surface. In the case of photocleavable *ortho*-nitrobenzyl SAMs on gold it was shown that a competing photoreduction of the NO_2 groups to NH_2 reduced the efficacy of photocleavage to $\approx$50% thus on silica we have a significant increase in yield.[44] As expected, the N 1s (NO_2) peak (Figure 2c) has almost completely

Table 1. Ellipsometry and contact angle data of the APMES SAM, after reaction with reagent **9** and finally after photolysis.

Surfaces	Ellipsometric thickness [Å]	Contact angle [°] advancing	receding
APMES	7 ± 1	78 ± 1	32 ± 1
APMES + **9**	19 ± 2	101 ± 2	58 ± 1
APMES + **9** after 2 h photolysis	10 ± 1	81 ± 1	41 ± 1

Table 2. Binding energy shift observed in the N 1s region.

Band	Chemical species	Binding energy [eV]
1A	NH_2	400.4
1B	NH_2/-$NHCO_2$-	400.4–400.8
2	NH_3^+	402.3
3	NO_2	406.6

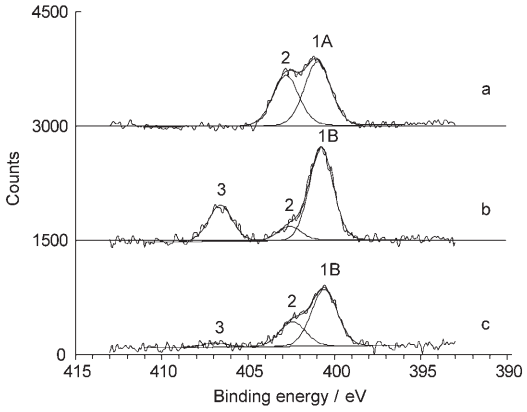

Figure 2. X-ray photoelectron spectra of the N 1s region a) APMES SAM, b) after reaction with reagent **9**, c) after irradiation at 365 nm for 3600 s.

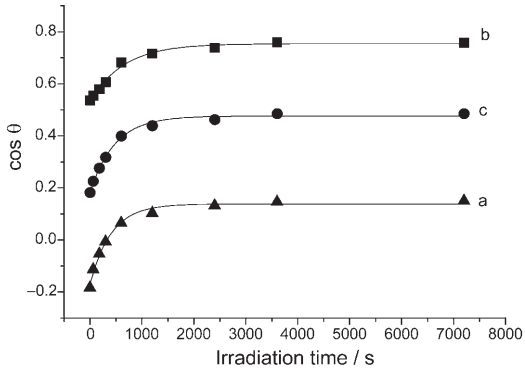

Figure 3. Contact angle variation during photolysis using soft UV light (365 nm, 7 mW cm^{-2}). a) Advancing water contact angle, b) receding water contact angle, and c) the average of the advancing and receding water contact angle. In cases (a) and (b) the lines are guides to the eye whilst in case (c) the line represents a fit to the data using the Cassie equation (see text).

action did not go 100%. The photocleavage reaction scheme is shown in Schem 2. Using the Cassie equation and the limiting values obtained from a pure APMES film and the unirradiated film we estimate that $\approx$25% of original tether disappeared at the end of the reaction. This is also consistent with the suggestion that the side reaction is the reduction of NO_2 to NH_2.

From the fit to the contact angle data we can estimate the rate constants for the photocleavage reaction, k_1, and the

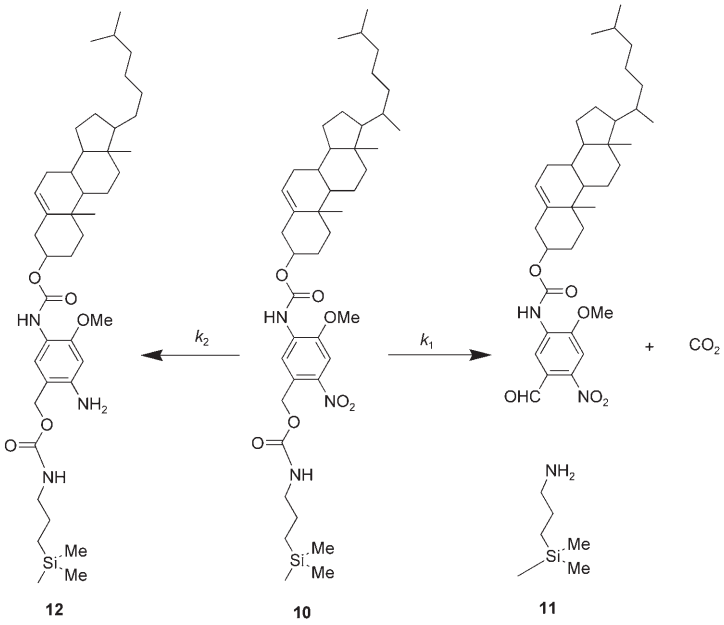

Scheme 2. The photocleavage process. By analogy with previous work the competing side reaction is identified as a reduction of the *ortho*-NO_2 to NH_2. The fact that this leads to a product which can no longer be photocleaved from the surface certainly indicates that the NO_2 is no longer present.

competing side reaction, k_2, to be $(1.5\pm0.1)\times10^{-3}\,s^{-1}$ and $(0.5\pm0.1)\times10^{-3}\,s^{-1}$, respectively.[44] The rate constant for photocleavage is significantly larger than that found for the thiol/gold system, k_1 for gold was $(0.33\pm0.05)\times10^{-3}\,s^{-1}$, while that of the competing side reaction is similar to that found on the gold-based system.[44]

Patterns can readily be formed by irradiation through a mask. Figure 4 shows an SEM image of a SAM photopatterned by using soft UV light (365 nm). The dark circles areas are where photolysis has occurred leaving regions of amine-functionalized surface; the bright regions show the tethered cholesterol moieties. The contrast is reversed from patterned fluorocarbon SAM.[43] This is due to reversal of the net dipole in the relevant SAMs.

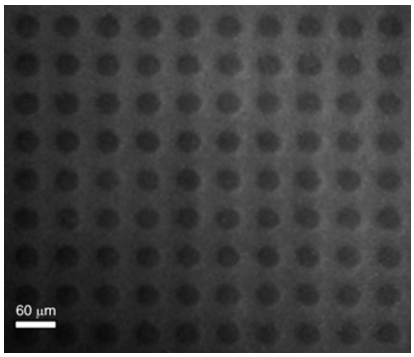

Figure 4. A scanning electron microscope (SEM) image of 30 μm diameter circles patterned surface. The dark regions correspond to areas where photodeprotection has occurred.

The patterned samples were imaged by friction mode AFM in air, which clearly shows 30 μm diameter circles of the amine surfaces (Figure 5a). Using an unmodified tip, the friction force observed on hydrophilic area of amine group was significantly higher than the friction force on the hydrophobic tether regions. Following incubation with SUVs (Figure 5b), the contrast due to the patterned SAM is not observed because the outer leaflet of the bilayer is the same as the lipid monolayer over the tether region. The white specks in Figure 5b are physically adsorbed, and in some cases partially ruptured, vesicles. Force volume imaging was then carried out, which did not show a significant difference in the adhesion force. However, analysis of the penetration distance (taken at the point of positive gradient in force-distance data over 90 μm^2 region of surface) shows two distributions (Figure 5c). The first, centered at 4.4 nm is consistent with the penetration of the lipid bilayer. A typical waveform in this region is shown as the dot plot in Figure 5d which shows a 4 nm transition followed by a small 1 nm compression. The second distribution was centered at 3.4 nm. A typical waveform in this region shown as the solid line in Figure 5d shows a 2 nm transition which is consistent with the penetration of the lipid monolayers, followed by a 2 nm compression of the underlying SAM. The area fraction corresponding to bilayer formation was calculated (from the areas of the Gaussian fits to the penetration distance distribution data) to be 30.5% which is in the range of 8.7 to 34.8% calculated as the fractional surface area of the amine pattern on the SAM.

Following incubation of the patterned SAMs with egg phosphatidylcholine (PC) vesicles (containing 1 mol% Texas Red-labeled 1,2-dihexadecanoyl-*sn*-glycero-3-phosphoethanolamine) fluorescence microscopy shows bright regions corresponding to lipid bilayer separated by darker regions in-between corresponding to areas of adsorbed lipid monolayer. The very bright specks are unruptured vesicles attached to the surface. In Figure 6a one of the bilayer regions has been partially photobleached. Monitoring the intensity recovery in this region (Figure 6b) we calculate the diffusion coefficient, D, to be $\approx0.14\pm0.05\,\mu m^2 s^{-1}$ and the mobile fraction of lipid to be only around 40%. This value of D is more than an order of magnitude lower than that observed for lipid bilayers adsorbed directly onto glass supports, $4.6\pm1.2\,\mu m^2 s^{-1}$[20] and approximately a factor of 2 lower than that observed for bilayer formed directly onto non-patterned APMES SAMs, ($D\approx0.36\pm0.15\,\mu m^2 s^{-1}$; Supporting Information, Figure S1). There are two points to note about this slow recovery. Firstly, in a typical FRAP experiment lipid diffusion is isotropic, permitting the diffusion of bleached and unbleached species equally rapidly in all directions. Here, however, the bleached region, B, consists of a bilayer portion B_1 and a lipid monolayer portion B_2. Diffusion to and from portion B_1 will be relatively rapid from region A, but much slower from regions B_2 and C. Lipid diffusion in the adsorbed lipid monolayer region is $\approx0.01\,\mu m^2 s^{-1}$ (see Supporting Information Figure S2), that is, over an order of magnitude lower than that found in the

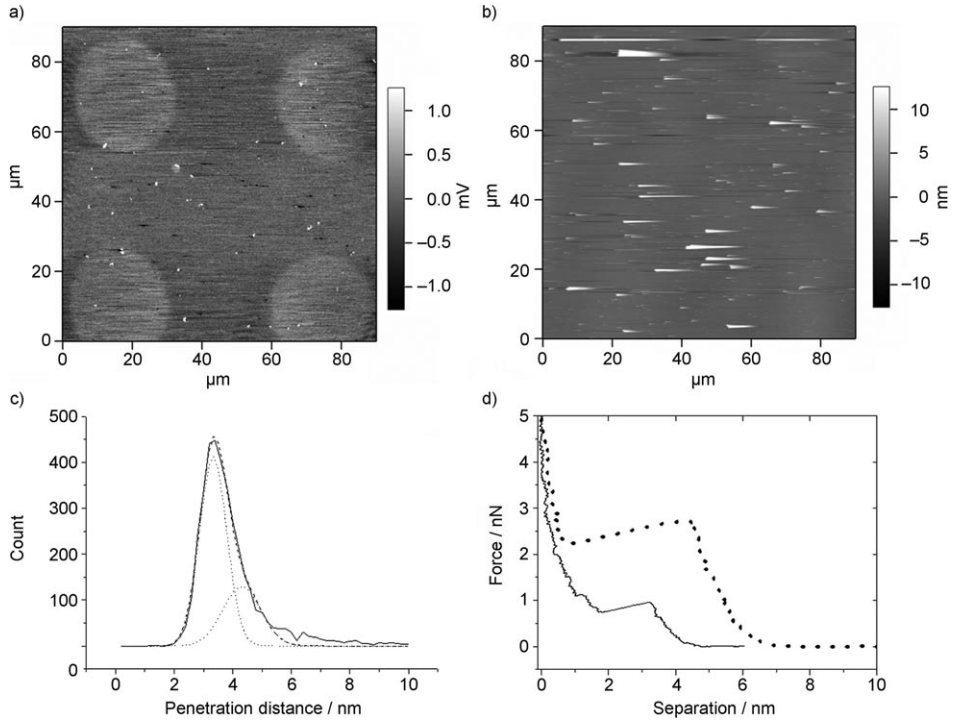

Figure 5. a) Friction mode AFM image of 30 μm-circle photopatterned SAM; b) tapping mode AFM image after lipid membrane formation; c) the histogram of penetration distance over 90 μm^2 region of surface (——). Dash and dot lines are Gaussian fits and sum of the two Gaussian fits, respectively; d) typical force curve for lipid bilayer regions (•••••) and for lipid monolayer–tether regions (——).

bilayer regions. The upper curve (Figure 6b) shows the result of a finite element analysis simulation of the expected recovery behavior based on the pattern geometry used experimentally and the diffusion coefficients determined from lipid bilayers on "pure" amine SAMs and adsorbed lipid monolayers on pure cholesterol tether surface. The faster recovery and higher mobile fraction obtained in the simulation curve than those from experimental curve implies a second factor for slow recovery, that is, the ≈25% remaining cholesterol tethers. In a typical bilayer on glass, the lipid in both leaflets is "bleached", and is assumed to have roughly the same diffusion constants. Here, however, only lipid in the out leaflet (upper surface) could be regarded as free to diffuse unrestricted. Whilst the lipid in the lower leaflet will encounter ≈25% coverage of immobile cholesterol tethers, which presents a significant restriction to lipid diffusion in the lower leaflet.

Conclusion

We have demonstrated that a surface can be formed by attaching cholesterol through photocleavable tether to an APMES SAM on silica. Subsequent photolysis regenerates the APMES surface. This system has a significantly better photolysis yield than equivalent thiol-on-gold SAMs. The functionalized surface can be patterned by exposing to 365 nm UV light through a mask. The resulting patterned surfaces can then be used to supported lipid bilayer arrays. The significant difference in diffusion coefficients between lipid bilayer and monolayer regions leads each of these regions to be effectively isolated from one another. This method for fabricating supported patterned lipid bilayers is very flexible and versatile, allowing to any required shape or size of lipid bilayer to be formed simply by changing the mask. Further it has the advantage over the μCP method,[29,30] that the patterned bilayers can be formed in fewer steps. Because it is applicable to silica substrates, the method also enables us to study the lipid bilayer by fluorescence microscopy which is difficult on gold substrates. The diffusion coefficient of patterned lipid bilayer was found to be significantly slower than that of lipid bilayer on glass. Most of this difference is attributable to the fact that it is supported over an amine-functionalized SAM.

Experimental Section

Materials: Dichloromethane 99.9% and toluene were supplied by Fisher scientific. 3-Aminopropyldimethylethoxysilane (APMES) was purchased from Fluorochem Limited. Diisoproylethylamine 99.5% was obtained from Sigma-Aldrich. Silicon substrates, supplied by Rockwood Electronic Materials, were cut into approximately 1.2 cm^2 from n-tpye doped, (100) wafers. Egg yolk phosphatidylcholine (egg PC) was purchased from Avanti Polar Lipids. Texas Red-labeled 1,2-dihexadecanoyl-*sn*-glycero-3-phosphoethanolamine triethylammonium salt (Texas Red DHPE) was purchased from Molecular Probes. Millipore Milli-Q water with a resistivity of 18.0 MΩ cm was used throughout.

Synthesis

4-Methoxy-3-nitrobenzaldehyde (2): 4-Methoxybenzaldehyde (**1**) (2.6 g, 2 mmol) was slowly added to nitric acid (70%, 20 mL) at room temperature, and the mixture stirred for a further 12 h. The reaction mixture was poured into ice water (50 mL). The resultant yellow solid was collected by filtration and washed by cold water, dried and purified by recrystallisation using ethyl acetate to afford the product (2.7 g, 90%) as pale yellow prisms. Further the product was authenticated by comparing the IR and ^1H NMR values with the authentic sample.[51]

3-Amino-4-methoxybenzaldehyde (3): Raney nickel (3 mL, 1.1 mmol, 50% slurry in water) was added to a stirred solution of 3-nitro-4-methoxybenzaldehyde (**2**; 1.8 g, 1 mmol) and ammonium chloride (1 g, 2 mmol) in distilled water (120 mL). The reaction mixture was heated under reflux for 2 h and cooled to room temperature. To this reaction mixture, ethyl acetate (20 mL) was added and the solution was stirred for 30 min. The reaction mixture was filtered, the organic layer was separated and the aqueous layer extracted with ethyl acetate (3×10 mL). The combined

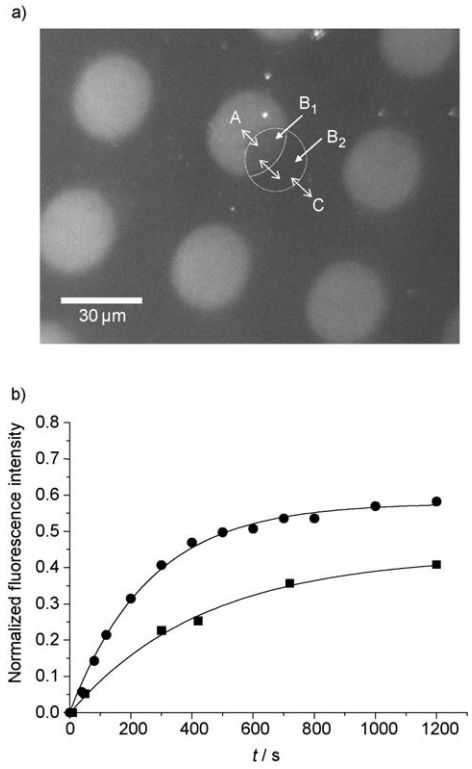

Figure 6. Lipid bilayer array on photopatterned surface: a) 30 μm diameter regions of bilayer separation by region of lipid monolayer. The dotted circle shows the area bleached. b) Fluorescence recovery after photobleaching (FRAP). Solid squares represent actual data, whilst the solid circles represent prediction based on modeling. From actual data, we calculate the diffusion coefficient, D, to be $\approx 0.14 \pm 0.05\ \mu m^2 s^{-1}$ and the immobile fraction of lipid to be only around 60%.

organic layers were dried over anhydrous magnesium sulfate. After filtration, the solvent was removed under reduced pressure to give a solid which was purified by flash chromatography on silica gel eluting with ethyl acetate/hexane 1:3 to afford **3** (1.2 g, 80%). M.p. 89.8°C; ^{1}H NMR (300 MHz, $CDCl_3$, 25°C, TMS): $\delta = 9.78$ (s, 1H; CHO), 7.27 (d, $J = 9.6$ Hz, 1H; ArH), 7.23 (s, 1H; ArH), 6.88 (d, $J = 9.6$ Hz, 1H; ArH), 3.99 (br, 2H; NH_2), 3.92 ppm (s, 3H; OMe); ^{13}C NMR (75 MHz, $CDCl_3$, 25°C, TMS): $\delta = 191.8$, 152.7, 137.3, 130.7, 123.9, 113.4, 110.0, 56.1 ppm; ESI-HRMS: m/z: calcd for $C_8H_9NO_2$: 151.0633 $[M]^+$, found: 151.0632; elemental analysis calcd (%) for $C_8H_9NO_2$: C 63.60, H 6.00, N 9.3; found: C 62.45, H 5.70, N 10.2.

3-Acetamido-4-methoxybenzaldehyde (4): Acetic acid (0.8, 1.2 mmol) was added to a stirred solution of 3-amino-4-methoxybenzaldehyde (**3**; 1.5 g, 1 mmol) in acetic anhydride (1.2 mL, 1.2 mmol). After 1 h of stirring, water (10 mL) was added and the aqueous layer extracted with ethyl acetate (3×20 mL).The combined organic layers were washed with brine (2×10 mL) followed by water (10 mL) and dried over anhydrous magnesium sulfate. After filtration, the solvent was removed under reduced pressure to give a solid which was purified by flash chromatography on silica gel eluting with ethyl acetate/hexane 1:4 to afford the product **4** (1.8 g, 95%). M.p. 106–107°C; ^{1}H NMR (300 MHz, $CDCl_3$, 25°C, TMS): $\delta = 9.90$ (s, 1H; CHO), 8.88 (s, 1H; ArH), 7.77 (s, 1H; NHCO), 7.65 (d, $J = 8.4$ Hz, 1H; ArH), 7.00 (d, $J = 8.4$ Hz, 1H; ArH), 3.98 (s, 3H; OMe), 2.23 ppm (s, 3H; COMe); ^{13}C NMR ($CDCl_3$, 25°C, TMS): $\delta =$ 191.5, 168.8, 152.7, 130.4, 128.6, 125.8, 122.1, 110.4, 56.5, 25.8 ppm; ESI-HRMS: m/z: calcd for $C_{10}H_{11}NO_3$+Na: 216.0631; found: 216.0635 $[M+Na]^+$; elemental analysis calcd (%) for $C_{10}H_{11}NO_3$: C 62.20, H 5.70, N 7.2; found: C 62.0, H 5.55, N 7.0.

5-Acetamido-4-methoxy-2-nitrobenzaldehyde (5): 3-Acetamido-4-methoxybenzaldehyde (**4**; 1.5 g, 0.77 mmol) was slowly added to nitric acid (70%, 15 mL) with stirring at room temperature, and the reaction mixture was stirred at room temperature for a further 12 h. The reaction mixture was poured into ice/water (30 mL). The resultant yellow solid was collected by filtration and washed with cold water, dried and purified by recrystallisation with ethyl acetate to afford **5** (1.3 g, 75%) as pale yellow prisms. M.p. 214–215°C; ^{1}H NMR (300 MHz, $CDCl_3$, 25°C, TMS): $\delta = 10.43$ (s, 1H; CHO), 8.98 (s, 1H; ArH), 7.97 (s, 1H; NHCO), 7.63 (s, 1H; ArH), 4.23 (s, 3H; OMe), 2.32 ppm (s, 3H; $COCH_3$); ^{13}C NMR (75 MHz, $[D_6]$DMSO, 25°C): $\delta = 188.9$, 170.0, 152.0, 145.5, 132.8, 124.3, 119.8, 107.4, 57.3, 24.4 ppm; ESI-HRMS: m/z: calcd for $C_{10}H_{10}N_2O_5$+Na: 261.0482, found: 261.0472 $[M+Na]^+$; elemental analysis calcd (%) for $C_{10}H_{10}N_2O_5$: C 50.40, H 4.20, N 11.80; found: C 49.4, H 3.95, N 12.0.

2-Nitro-5-amino-4-methoxybenzaldehyde (6): 5-Acetamido-4-methoxy-2-nitrobenzaldehyde (**5**; 1.1 g, 0.5 mmol) was added to hydrochloric acid (2 N, 10 mL) with stirring at room temperature, and the reaction mixture was heated under reflux for 3 h. The reaction mixture was extracted with ethyl acetate (3×10 mL) and the combined organic layers were dried over anhydrous magnesium sulfate. After filtration, the solvent was removed under reduced pressure to give a solid which was purified by flash chromatography on silica gel eluting with ethyl acetate/hexane 1:1 to afford **6** (0.74 g, 70%). M.p. 193–194°C; ^{1}H NMR (300 MHz, $CDCl_3$, 25°C, TMS): $\delta = 10.46$ (s, 1H; CHO), 7.59 (s, 1H; ArH), 7.10 (s, 1H; ArH), 4.64 (br s, 2H; NH_2) 4.01 (s, 3H; OMe), 2.32 ppm (s, 3H; $COCH_3$); ^{13}C NMR (75 MHz, $[D_6]$acetone, 25°C): $\delta = 190.0$, 149.0, 145.4, 140.0, 129.7, 111.8, 107.7, 57.2 ppm; ESI-HRMS (negative mode) calc. for $(M\text{-}H)^-$:195.0411, found: 195.0412; elemental analysis calc (%) for $C_8H_8N_2O_4$: C 48.97, H 4.08, N 14.28; found: C 49.0, H 4.25, N 14.10.

Carbamate 7: Diisopropylethylamine (0.52 mL, 0.3 mmol) and a few mg of DMAP were added to a stirred solution of 2-nitro-5-amino-4-methoxybenzaldehyde (**6**; 0.39 g, 0.2 mmol), cholesteryl chloroformate (0.99 g, 0.22 mmmol) in anhydrous toluene (40 mL). The reaction mixture was heated under reflux overnight followed by removal of solvent under reduced pressure resulting in a reddish-brown residue. The residue was purified by flash chromatography on silica gel eluting with 5% ethyl acetate/hexane to afford **7** (0.66 g, 55%) as a yellow solid. M.p. 231–232°C; ^{1}H NMR (300 MHz, $CDCl_3$, 25°C, TMS): $\delta = 10.41$ (s, 1H; CHO), 8.71 (s, 1H; NHCO), 7.60 (s, 1H; ArH), 7.40 (s, 1H; ArH), 5.40 (d, $J = 5.4$ Hz, 1H; vinyl cholesteryl), 4.61 (m, 1H; O-CH- of cholesteryl), 4.05 (s, 3H; OMe), 0.85–2.47 (m, 22H; cholesteryl), 1.03 (s, 6H; cholesteryl), 0.92 (d, $J = 6.6$ Hz, 3H; cholesteryl), 0.87 (d, $J = 7.8$ Hz, 6H; cholesteryl), 0.68 ppm (s, 6H; cholesteryl); ^{13}C NMR(75 MHz, $CDCl_3$, 25°C, TMS): $\delta = 187.9$, 152.4, 150.1, 144.4, 139.6, 133.8, 126.7, 123.5, 117.5, 106.4, 76.5, 57.1, 57.0, 56.5, 50.4, 42.7, 40.1, 39.9, 38.6, 37.3, 36.9, 36.5, 36.2, 32.3, 28.6, 28.4, 28.3, 24.6, 24.2, 23.2, 22.9, 21.4, 19.7, 19.1, 12.2 ppm; ESI-HRMS (negative mode): m/z: calcd for $C_{36}H_{51}N_2O_6$: 607.3748 $[M^-]$, found: 607.3753; elemental analysis calcd (%) for $C_{36}H_{52}N_2O_6$: C 71.05, H 8.63, N 4.60; found: C 69.9, H 8.65, N 4.45.

Carbamate 8: Sodium borohydride (0.11 g, 0.3 mmol) was added to a solution of the carbamate (**7**) (0.6 g, 0.1 mmol) in anhydrous THF (10 mL) and the mixture stirred for 10 h. The reaction was quenched by addition of water (10 mL). The organic layer was separated and the aqueous layer was extracted with ethyl acetate (3×10 mL).The combined organic layers were dried over anhydrous magnesium sulfate. After filtration, the solvent removed under reduced pressure to give a solid which was purified by flash chromatography eluting with dichloromethane to afford **8** (0.54 g, 90%) as yellow solid. M.p. 211–212°C; ^{1}H NMR (300 MHz, $CDCl_3$, 25°C, TMS): $\delta = 8.48$ (s, 1H; NHCO), 7.68 (s, 1H; ArH), 7.42 (s, 1H; ArH), 5.41 (d, $J = 5.4$ Hz, 1H; vinyl cholesteryl), 4.91 (d, $J = 6.9$ Hz, 2H; benzylic -CH_2), 4.61 (m, 1H; O-CH- of cholesteryl), 3.97 (s, 3H; OMe), 2.70 (t, $J = 14.0$, 7.0 Hz, 1H; benzylic -OH), 0.85–2.47 (m, 22H; cholesteryl), 1.03 (s, 6H; cholesteryl), 0.92 (d, $J = 6.6$ Hz, 3H; cholesteryl), 0.87 (d, J = 7.8 Hz, 6H; cholesteryl), 0.68 ppm (s, 6H; cholesteryl); ^{13}C NMR (75 MHz, $CDCl_3$, 25°C, TMS): $\delta = 152.7$, 146.5, 141.4, 139.6, 134.1, 132.5, 123.4, 118.3, 107.3, 76.2, 63.4, 57.1, 57.0, 56.5, 50.4, 42.7, 40.1, 39.9, 38.6, 37.3, 36.9, 36.5, 36.2, 32.3, 28.6, 28.4, 28.3, 24.6, 24.2, 23.2, 22.9, 21.4, 19.7, 19.1, 12.2 ppm; ESI-HRMS (negative mode): m/z: calcd for

$C_{36}H_{53}N_2O_6$: 609.3909 [M^-], found: 609.3915; elemental analysis calcd (%) for $C_{36}H_{54}N_2O_6$: C 70.81, H 8.85, N 4.59; Found: C 70.75, H 8.95, N 4.45.

Reagent 9: *N*,*N*′-Disuccinimidyl carbonate (0.15 g, 0.058 mmol), triethylamine (0.23 mL,0.17 mmol) were added to a solution of the carbamate **8** (0.3 g, 0.05 mmol) in anhydrous DMF (5 mL), and the reaction mixture was stirred for 5 h. Water (10 mL) was added. The organic layer was separated and the aqueous layer was extracted with ethyl acetate (3×10 mL) and the combined organic layers were dried over anhydrous magnesium sulfate. After filtration, the solvent removed under reduced pressure to give a solid which was purified by flash chromatography eluting with dichloromethane to afford **9** (318 mg, 85%) as yellow powder. M.p. 236.8 °C; ^{1}H NMR ($CDCl_3$, 25 °C, TMS_i: δ = 8.49 (s, 1H; NHCO), 7.73 (s, 1H; ArH), 7.42 (s, 1H; ArH), 5.72 (s, 2H; benzylic CH_2), 5.41 (d, J = 5.4 Hz, 1H; vinyl cholesteryl), 4.65 (m, 1H; O-CH- of cholesteryl), 3.99 (s, 3H; OMe), 2.84 (s, 4H; -N-CH_2-CH_2-N-), 0.85–2.47 (m, 22H; cholesteryl), 1.03 (s, 6H; cholesteryl), 0.92 (d, J = 6.6 Hz, 3H; cholesteryl), 0.87 (d, J = 7.8 Hz, 6H; cholesteryl), 0.68 ppm (s, 6H; cholesteryl); ^{13}C NMR (75 MHz, $CDCl_3$, 25 °C, TMS): δ = 168.7, 152.6, 151.5, 147.2, 141.2, 139.7, 134.2, 124.6, 123.4, 117.6, 107.5, 76.5, 63.4, 57.1, 57.0, 56.5, 50.4, 42.7, 40.1, 39.9, 38.6, 37.3, 36.9, 36.5, 36.2, 32.3, 25.8, 28.6, 28.4, 28.3, 24.6, 24.2, 23.2, 22.9, 21.4, 19.7, 19.1, 12.2 ppm; ESI-HRMS (negative mode): m/z: calcd for $C_{41}H_{56}N_3O_{10}$: 750.3971 [M^-]; found: 750.3998.

Substrate cleaning: Silicon substrates were cleaned by ultrasonication in dichloromethane for 15 min, dried under a stream of nitrogen, and rinsed in Milli-Q water before being immersed in Piranha solution (70:30, v/v, H_2SO_4/H_2O_2; **CAUTION**: Piranha solution reacts violently with organic materials and should be treated with great care) for 5 min. The substrates were rinsed in Milli-Q water and dried under nitrogen. The water contact angles were typically much less than 5° for freshly cleaned substrates.

Silanization: The clean dried substrates were immersed into anhydrous toluene solution with 1% APMES under a nitrogen atmosphere for 18 h at room temperature. After silanization they were washed with toluene and CH_2Cl_2, and dried under nitrogen. The silanized substrates were used immediately.

APMES Derivatization: The APMES SAMs were immediately placed in anhydrous CH_2Cl_2 containing a 20 mM solution of the reagent **9** (under a nitrogen atmosphere) and 1% (by volume) diisoproylethylamine added. The solution was maintained at room temperature, 22 °C, and stored in the dark. After 6 h, the samples were removed, rinsed with CH_2Cl_2, ultrasonicated in CH_2Cl_2, and dried under nitrogen.

UV irradiation of the functionalized surface: A 365 nm UV lamp (Blak-Ray model B 100 AP) with a nominal power, at the sample, of 7 mW cm^{-2} was used to irradiate the samples. After the UV exposure, samples were rinsed with CH_2Cl_2, followed by Milli-Q water, and finally dried under nitrogen. The emission spectrum of the lamp displayed three prominent lines, 309, 331, and 365 nm, with integrated intensities of 0.005:0.03:1, respectively. Photopatterning was achieved by irradiation of samples through a chromium/quartz mask, for one hour. Patterned samples were rinsed with CH_2Cl_2, followed by Milli-Q water, and finally dried under a stream of nitrogen.

Wetting measurements: Contact angles were measured using a First Ten Angstroms (FTA4000) instrument. Advancing and receding contact angles were obtained using the "Dynamic Contact Angle Analyzer". Measurements were made on at least three different points on each sample.

X-ray photoelectron spectroscopy: Spectra were obtained using a Thermo VG ESCALAB 250 with a base pressure maintained below 5×10^{-9} mbar during acquisition. A monochromated $Al_{K\alpha}$ X-ray source (15 kV 150 W) irradiated the samples, with a spot diameter of approximately 0.5 mm. The spectrometer was operated in Large Area XL magnetic lens mode, using pass energies of 150 and 20 eV for survey and detailed scans, respectively. Spectra were obtained with an electron takeoff angle of 90°. High-resolution spectra were fitted using Avantage (Thermo VG software) peak fitting algorithms.

Ellipsometry: A Jobin-Yvon UVISEL spectroscopic ellipsometer was used to measure the thickness of the SAMs. The wavelength was varied between 300 and 800 nm in steps of 15 nm. DeltaPsi2 software was used to model and fit the acquired data assuming a simple three-layer system. Values for the base layer (silicon dioxide) were obtained from a freshly cleaned silicon substrate. The SAM was modelled as a transparent thin film using the Cauchy approximation, $n(\lambda) = A + \frac{B\cdot10^4}{\lambda^2} + \frac{C\cdot10^9}{\lambda^4}$ and $k(\lambda) = 0$. Where λ is the wavelength in units of nanometres and A, B and C are the Cauchy parameters dependant on optical properties of the material. Parameter, A, was restricted to a value of 1.46 and parameters B and C were allowed to vary between 0–1 nm^2 and 0–0.2 nm^4, respectively. The ambient, air, was assumed to have n = 1 and k = 0. At least six ellipsometric measurements were made per sample (and on more than one sample of each type).

Scanning electron microscopy (SEM): SEM images were obtained using a Zeiss Gemini 1500 UHV SEM attached to an Omicron Nanoprobe (Germany) with EHT of 10 kV and a probe current of 100 pA (working distance approx. 13 mm).

Vesicle preparation: Small unilamellar vesicles (SUVs) were prepared by tip sonication. 5 mg of egg PC containing 1 mol% TR-DHPE chloroform solution was dried under nitrogen in a small glass vial over night. The dried egg PC film was then hydrated in 1 mL 0.1 M KCl by vortexing. The cloudy solution was tip-sonicated at less than 5 °C until the solution became clear. In order to remove any metal particulates from the tip, the clear solution was centrifuged at a speed of 13000 rev per s for 30 min. Finally, the vesicle solution was diluted to egg PC concentration of 2 mg mL^{-1}.

Fluorescence microscopy and Fluorescence recovery after photobleaching (FRAP): A Nikon E600 fluorescence microscope equipped with a Hamamatsu (ORCA-ER) digital camera was used to image the patterned bilayers and to carry out FRAP measurements. Image-Pro Express data acquisition software (Media Cybernetics) was used to obtain and analyze images. The lateral diffusion coefficient (D) was calculated from D = 0.224 $\omega^2/t_{1/2}$, where ω is the radius of the bleached spot and $t_{1/2}$ is the half-life of the fluorescence recovery.[49,50]

Atomic force microscopy (AFM) measurement: AFM images were taken using an Asylum Research Inc. MFP-3D, using Veeco NPS cantilevers having nominal spring constants of 0.06 N m^{-1}. Friction mode images were taken in contact mode in air and tapping mode images were taken in Pipes buffer, at pH 7, with a cantilever resonant frequency of 9 kHz. Force volume images were taken in Pipes buffer, at pH 7, and with an approach rate of 400 nm s^{-1} (this value was chosen to minimizing the effect of approach velocity of the tip to the penetration distance[52]) using a 64 by 64 unit grid and analysed using an in-house program.

Acknowledgement

We thank EPSRC for financial support: GR/S87195/01 and EP/C006755/1.

[1] M. Montal, P. Mueller, *Proc. Natl. Acad. Sci. USA* **1972**, *69*, 3561–3566.
[2] P. Mueller, D. O. Rudin, H. T. Tien, W. C. Wescott, *Nature* **1962**, *194*, 979–980.
[3] Z. Leonenko, E. Finot, D. Cramb, *Biochim. Biophys. Acta* **2006**, *1758*, 487–492.
[4] S. Lingler, I. Rubinstein, W. Knoll, A. Offenhausser, *Langmuir* **1997**, *13*, 7085–7091.
[5] R. Naumann, S. M. Schiller, F. Giess, B. Grohe, K. B. Hartman, I. Karcher, I. Koper, J. Lubben, K. Vasilev, W. Knoll, *Langmuir* **2003**, *19*, 5435–5443.
[6] E. Sackmann, *Science* **1996**, *271*, 43–48.
[7] E. Sackmann, *Mol. Biotechnol.* **2000**, *74*, 135–136.
[8] E. Sackmann, M. Tanaka, *Trends Biotechnol.* **2000**, *18*, 58–64.

[9] S. M. Schiller, R. Naumann, K. Lovejoy, H. Kunz, W. Knoll, *Angew. Chem.* **2003**, *115*, 219–222; *Angew. Chem. Int. Ed.* **2003**, *42*, 208–211.
[10] M. Tanaka, E. Sackmann, *Nature* **2005**, *437*, 656–663.
[11] S. Terrettaz, M. Mayer, H. Vogel, *Langmuir* **2003**, *19*, 5567–5569.
[12] S. Terrettaz, H. Vogel, *MRS Bull.* **2005**, *30*, 207–210.
[13] L. M. Williams, S. D. Evans, T. M. Flynn, A. Marsh, P. F. Knowles, R. J. Bushby, N. Boden, *Langmuir* **1997**, *13*, 751–757.
[14] B. A. Cornell, V. L. B. BraachMaksvytis, L. G. King, P. D. J. Osman, B. Raguse, L. Wieczorek, R. J. Pace, *Nature* **1997**, *387*, 580–583.
[15] H. Bayley, P. S. Cremer, *Nature* **2001**, *413*, 226–230.
[16] O. Worsfold, N. H. Voelcker, T. Nishiya, *Langmuir* **2006**, *22*, 7078–7083.
[17] M. A. Cooper, *J. Mol. Recognit.* **2004**, *17*, 286–315.
[18] J. T. Groves, *Curr. Opin. Drug Discovery Dev.* **2002**, *5*, 606–612.
[19] P. S. Cremer, T. L. Yang, *J. Am. Chem. Soc.* **1999**, *121*, 8130–8131.
[20] J. T. Groves, S. G. Boxer, *Biophys. J.* **1995**, *69*, 1972–1975.
[21] J. T. Groves, N. Ulman, S. G. Boxer, *Science* **1997**, *275*, 651–653.
[22] J. T. Groves, N. Ulman, P. S. Cremer, S. G. Boxer, *Langmuir* **1998**, *14*, 3347–3350.
[23] B. L. Jackson, J. T. Groves, *Langmuir* **2007**, *23*, 2052–2057.
[24] L. A. Kung, L. Kam, J. S. Hovis, S. G. Boxer, *Langmuir* **2000**, *16*, 6773–6776.
[25] K. Morigaki, T. Baumgart, A. Offenhausser, W. Knoll, *Angew. Chem.* **2001**, *113*, 184–186; *Angew. Chem. Int. Ed.* **2001**, *40*, 172–174.
[26] K. Morigaki, T. Baumgart, U. Jonas, A. Offenhausser, W. Knoll, *Langmuir* **2002**, *18*, 4082–4089.
[27] C. K. Yee, M. L. Amweg, A. N. Parikh, *J. Am. Chem. Soc.* **2004**, *126*, 13962–13972.
[28] C. K. Yee, M. L. Amweg, A. N. Parikh, *Adv. Mater.* **2004**, *16*, 1184–1189.
[29] A. T. A. Jenkins, R. J. Bushby, N. Boden, S. D. Evans, P. F. Knowles, Q. Y. Liu, R. E. Miles, S. D. Ogier, *Langmuir* **1998**, *14*, 4675–4678.
[30] A. T. A. Jenkins, N. Boden, R. J. Bushby, S. D. Evans, P. F. Knowles, R. E. Miles, S. D. Ogier, H. Schonherr, G. J. Vancso, *J. Am. Chem. Soc.* **1999**, *121*, 5274–5280.
[31] X. H. Han, K. Critchley, L. Zhang, S. N. D. Pradeep, R. J. Bushby, S. D. Evans, *Langmuir* **2007**, *23*, 1354–1358.
[32] Y. L. Cheng, N. Boden, R. J. Bushby, S. Clarkson, S. D. Evans, P. F. Knowles, A. Marsh, R. E. Miles, *Langmuir* **1998**, *14*, 839–844.
[33] L. J. C. Jeuken, S. D. Connell, P. J. F. Henderson, R. B. Gennis, S. D. Evans, R. J. Bushby, *J. Am. Chem. Soc.* **2006**, *128*, 1711–1716.
[34] L. M. Williams, S. D. Evans, T. M. Flynn, A. Marsh, P. F. Knowles, R. J. Bushby, N. Boden, *Supramol. Sci.* **1997**, *4*, 513–517.
[35] J. H. Moon, J. W. Shin, S. Y. Kim, J. W. Park, *Langmuir* **1996**, *12*, 4621–4624.
[36] I. George, P. Viel, C. Bureau, J. Suski, G. Lecayon, *Surf. Interface Anal.* **1996**, *24*, 774–780.
[37] H. L. Cabibil, V. Pham, J. Lozano, H. Celio, R. M. Winter, J. M. White, *Langmuir* **2000**, *16*, 10471–10481.
[38] R. R. Sahoo, A. Patnaik, *J. Colloid Interface Sci.* **2003**, *268*, 43–49.
[39] D. Kowalczyk, S. Slomkowski, M. M. Chehimi, M. Delamar, *Int. J. Adhes. Adhes.* **1996**, *16*, 227–232.
[40] J. H. Moon, J. H. Kim, K. Kim, T. H. Kang, B. Kim, C. H. Kim, J. H. Hahn, J. W. Park, *Langmuir* **1997**, *13*, 4305–4310.
[41] Y. C. Liu, R. L. Mccreery, *J. Am. Chem. Soc.* **1995**, *117*, 11254–11259.
[42] If we assume that there are x_0 amine groups on the surface prior to step 1 (Figure 1) and that following the reaction the NO_2 signal, y, is proportional to the number of reacted amines. Then the reaction yield is given by y/x_0, where x_0 can be determined from the total amine signal (after attachment), z, which is given by x_0+y because one reacted reagent **9** introduced one NH group. Thus the yield is given by $y/(z-y)$.
[43] K. Critchley, J. P. Jeyadevan, H. Fukushima, M. Ishida, T. Shimoda, R. J. Bushby, S. D. Evans, *Langmuir* **2005**, *21*, 4554–4561.
[44] K. Critchley, L. Zhang, H. Fukushima, M. Ishida, T. Shimoda, R. J. Bushby, S. D. Evans, *J. Phys. Chem. B* **2006**, *110*, 17167–17174.
[45] J. Nakanishi, Y. Kikuchi, T. Takarada, H. Nakayama, K. Yamaguchi, M. Maeda, *J. Am. Chem. Soc.* **2004**, *126*, 16314–16315.
[46] M. C. Pirrung, *Angew. Chem.* **2002**, *114*, 1326–1341; *Angew. Chem. Int. Ed.* **2002**, *41*, 1276–1289.
[47] E. Besson, A. M. Gue, J. Sudor, H. Korri-Youssoufi, N. Jaffrezic, J. Tardy, *Langmuir* **2006**, *22*, 8346–8352.
[48] A. B. D. Cassie, S. Baxter, *Trans. Faraday Soc.* **1944**, *40*, 0546–0550.
[49] D. M. Soumpasis, *Biophys. J.* **1983**, *41*, 95–97.
[50] L. Q. Zhang, M. L. Longo, P. Stroeve, *Langmuir* **2000**, *16*, 5093–5099.
[51] J. A. R. Rodrigues, R. A. Abramovitch, J.D.F de Sousa, G. C. Leiva, *J. Org. Chem.*, **2004**, *69*, 2920–2928.
[52] V. Franz, S. Loi, H. Muller, E. Bamberg, H. H. Butt, *Colloids Surf. B* **2002**, *23*, 191–200.

Received: April 3, 2007
Published online: July 4, 2007

